

## Magnetohydrodynamic simulation for plasma focus devices

M. M. MASOUD<sup>†</sup>, H. A. EL-GAMAL<sup>†</sup>, H. A. EL-TAYEB<sup>†</sup>, M. A. HASSOUBA<sup>‡</sup>  
and M. A. ABD AL-HALIM<sup>\*‡</sup>

<sup>†</sup>Nuclear Research Centre, Atomic Energy Authority, Cairo, Egypt

<sup>‡</sup>Physics Department, Faculty of Science, Benha University, Benha, Egypt

(Received 3 August 2007)

To overcome the discontinuity between the axial phase and the radial phase in the plasma focus, a new model (the Masoud model) has been developed. It is assumed that, according to the snowplough model, the radial phase moves in the angular direction with continuity between the axial and the radial phases. This model is based on the introduction of an angle of motion in all equations of motion and circuit. Then, the plasma sheath position and velocity were calculated numerically from the previous equations. A slug model has been used to calculate the shock wave velocity, and hence the electron temperature. Values of the discharge current, the axial speed, the axial position, the spike voltage, the radial piston speed, the radial piston position, the plasma column length and the plasma temperature have been obtained using the new model. The values calculated by using this model show good agreement with the published experimental results.

*Keywords:* Plasma focus; Lee model; Snowplough model; Slug model

### 1. Introduction

It has been found that the properties of plasma focus devices can be described by many closely correlated parameters, which are found empirically [1] and calculated theoretically [2]. To obtain optimum conditions, matching between a power supply and an electrode system, between a material and the dimensions of the insulator and the electrodes, and between the gas pressure and controlled homogeneous ignition should be ensured. Maxon and Eddleman [3] have developed a two-dimensional magnetohydrodynamic code to describe plasma focus experiments. They studied the shock wave in both the rundown phase and the radial phase. They reached good agreement between the calculated values of the plasma velocity, the ion temperature and the mass loss during the rundown phase with the experimental results. Potter [4] applied the slug model for the formation of a pinch by a strong shock wave, in which the pinch radius is related to the wall radius and is independent of the applied current. Lee [5, 6] developed his model of the plasma focus with a complete description of the plasma focus dynamics in the axial and in the radial phases. Potter used the snowplough model to derive

---

\*Corresponding author. Email: ma\_halim74@yahoo.com

the equation of motion and solved this equation numerically in the axial phase, taking into account the circuit equation to find the velocity and the position of the axial plasma sheath.

Lee [6] obtained a variation in the circuit current with the discharge time and used the shock wave properties to obtain the plasma temperature and the axial shock velocity. Lee [5, 7] used the slug model in the radial phase to calculate the radial shock speed and the radial piston speed by using the adiabatic law. By using the plasma circuit equation, Lee *et al.* [8] calculated the voltage across the tube, the variation in the axial kinetic energy and the current.

An updated version of this physical model was proposed by Lee [9] in his work on the sequential plasma focus. A mass factor and a current factor were included for the axial phase of the three phases considered.

Based on the corona model and experimental results, Lee and co-workers [10] developed a model of the radiative plasma focus by calculating the energy transfer in the plasma focus. A reflected shock phase and a radiative phase were also added to the model to simulate the X-ray emission from the plasma focus [11]. Lee and Serban [12] and Lee [13] also calculated the dimensions and the lifetime of the pinch.

Zakaullah *et al.* [14] used the previous model to obtain the optimum values of the parameters affecting focusing. They studied the effects of the ratio of the inner electrode radius to the outer electrode radius, the ratio of the inner electrode length to its radius, the insulator length, the external inductance, the gas pressure, the capacitance of the capacitor bank, and the charging voltage.

Moreno *et al.* [15] investigated another plasma focus model derived from a thermonuclear model. It was applied successfully to explain the variation in the neutron yield with a change in the gas pressure in chambers filled with deuterium, the current evolution, and the geometrical parameters of electrodes. Moreno *et al.* [15] assumed that the current sheath in the form of conical segments was moving at a certain angle and that each plasma segment accelerated by the Lorentz force moved normal to its surface.

In spite of the excellent agreement between the results calculated by the Lee model [5–12] and the results of experimental measurements, there are still some points to be considered.

- (i) The continuity between the plasma velocity in the axial phase and the plasma velocity in the radial phase (where the last step of the calculated axial velocity in the axial phase is greatly different from the first step of the calculated axial (elongation) velocity in the radial phase).
- (ii) The values calculated when the current is low are somewhat non-realistic for all parameters, and the procedure cannot continue in the cases of negative current.
- (iii) In the slug model, the radial plasma velocity is stopped in the fourth phase at 0.05 of the inner electrode radius not because of the corrected end point of the slug model.
- (iv) The current and voltage waveforms for some parameters have some non-realistic values.
- (v) The insertion of anomalous resistivity disturbs the values of current and voltage.
- (vi) The dependence of the shock wave velocity on the discharge current is not valid for small current values.
- (vii) Under some conditions, the model gives some oscillatory values and seems unstable during drastic abrupt changes in all characteristics caused by small changes in the system parameters.

## 2. Theoretical aspects and results of the new proposed model

We have developed a new model (the Masoud model) for the plasma focus, which is divided into five phases: an axial phase, a radial inward shock wave phase, a radial reflected shock phase, a radiative phase and an expanded column axial phase.

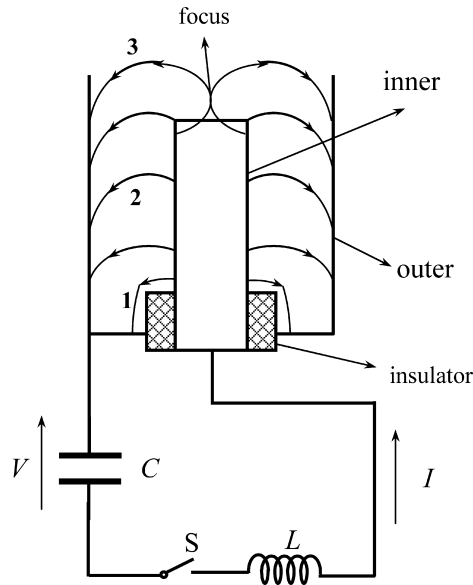


Figure 1. A plasma focus device.

The Mather-type plasma focus consists of two cylindrical electrode systems. A typical electric circuit of the plasma focus system is shown in figure 1. A capacitor bank of capacitance  $C$  is discharged through a circuit inductance  $L$ , a switch  $S$  and a discharge chamber. Two coaxial electrodes are insulated from each other. When the switch  $S$  is closed, the charging voltage  $V$  is applied across the insulator. During the ignition phase (1 in figure 1), a breakdown occurs and an axial symmetric current sheath is formed. Then the current increases and the sheath moves under the Lorentz force towards the open end (the ‘rundown’ phase) (2 in figure 1). After that, the sheath turns radial to the centre of the system (the ‘focus’ phase) (3 in figure 1) and is compressed on the axis [1].

### 2.1 Axial phase

In this phase, the snowplough model is used to study the motion of the plasma sheath. It is considered that the current sheath is planar and perpendicular to the accelerator axis. It is also considered that the Lorentz force ( $\mathbf{J} \times \mathbf{B}$ ) acting on the current sheath equals the rate of a change in the linear momentum of the moving sheath. It is assumed that the gas inside the sheath that swept upwards cannot penetrate the sheath, which acts like a solid piston [16, 17]. According to the snowplough model [18, 19], it is supposed that the density of the current sheath is equal to the integral density of the gas through which that sheath moves and where the shock wave preionizes the working gas on the front of the wave [20, 21].

In the discharge region, one can distinguish three characteristic zones [20, 22, 23], as is shown in figure 2. The regions are a magnetic piston next to the insulator, a current sheath region between the piston edge and the shock wave, and an undisturbed gas in the front part of the electrode system.

### 2.2 Radial phase

At the end of the axial phase, the current sheath begins to move in the radial direction owing to a deflection of a component of the electric current from the radial direction to the axial direction.

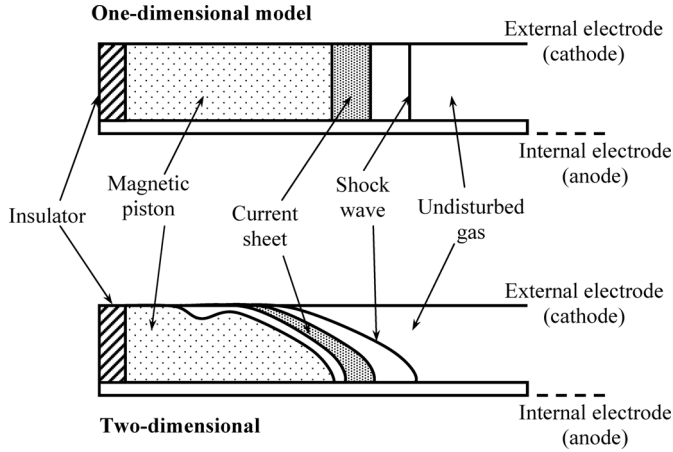


Figure 2. Schematic pattern of the discharge region.

To keep the continuity of the plasma sheath motion between the axial and radial phases, in our model it is considered that, the motion of the plasma sheath will be spherical in shape depending on the snowplough model rather than the slug model. Therefore, the slug model can be used to calculate the shock wave parameters and the plasma temperature. The configuration used is shown in figure 3 where the current  $I_r$  flows in the radial direction and the magnetic field  $B_\phi$  is in the azimuth direction so that the Lorentz force  $F_\theta$  deflects the sheath to an angle  $\theta$  and the energy is  $E = \frac{1}{2} L_T I^2$ . The magnetic force  $F_1$  acting on the current sheath can be deduced, for simplicity, by using the following equation:

$$F_1 = \frac{I^2 f_c^2 L_T}{2(Z_0 + r\theta)} \tag{1}$$

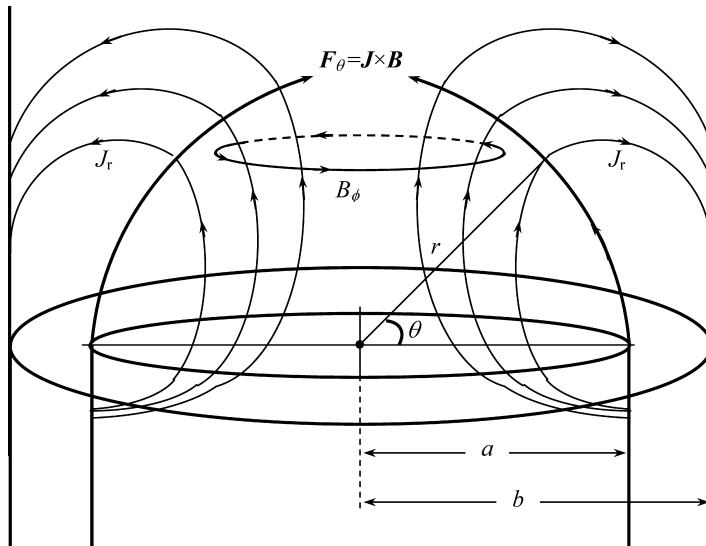


Figure 3. Suggested diagram of the radial phase in the plasma focus system.

The plasma inductance  $L_r$  in the radial area only is

$$L_r = \frac{\Phi_r}{I} = \frac{\mu z_f \ln[b/(r \cos \theta)]}{2\pi}, \quad (2)$$

where  $z_f$  is the position of the axial plasma current sheath.

The plasma inductance in the radial phase is obtained from the total magnetic flux per unit length as

$$\Phi_r' = \int_{r \cos \theta}^b B \, dr = \int_{r \cos \theta}^b \frac{\mu f_c}{2\pi r} \, dr = \frac{\mu f_c \ln[b/(r \cos \theta)]}{2\pi}. \quad (3)$$

Hence

$$\Phi_r = \Phi_r' z_f = \frac{\mu f_c z_f \ln[b/(r \cos \theta)]}{2\pi}, \quad (4)$$

where

$$\varepsilon = L_r \frac{dI}{dt} + I \frac{dL_r}{dt} = \frac{d\Phi_r}{dt}. \quad (5)$$

By differentiating equation (4) we have

$$\varepsilon = \frac{\mu f_c z_f \ln[b/(r \cos \theta)]}{2\pi} \frac{dI}{dt} + I \frac{d}{dt} \left( \frac{\mu f_c z_f \ln[b/(r \cos \theta)]}{2\pi} \right). \quad (6)$$

By comparing equations (5) and (6), we obtain that the plasma inductance  $L_r$  in the radial part only is

$$L_r = \frac{\Phi_r}{I} = \frac{\mu f_c z_f \ln[b/(r \cos \theta)]}{2\pi} \quad (7)$$

and

$$\frac{dL_r}{dt} = \frac{\mu f_c \{(dz_f/dt) \ln[b/(r \cos \theta)] + z_f \dot{\theta} \tan \theta\}}{2\pi}, \quad (8)$$

where the total plasma inductance in the radial phase is  $L_T = L_a + L_r$ .

It is considered that the plasma moves, as shown in figure 3, as a cylinder of the radius  $r \cos \theta$  expanding in the axial direction and compressed in the radial direction. So, the force is equal to the rate of change in the momentum of the current sheath at the angle  $\theta$  as follows:

$$F_2 = \frac{d(mv_\theta)}{dt} = \frac{d[(m_a + m_r)r\dot{\theta}]}{dt};$$

then

$$F_2 = \frac{d}{dt} \left( \{\rho f_m \pi (b^2 - a^2) z_0 + \rho f_m \pi r \sin \theta [b^2 - (a^2 \cos^2 \theta)]\} r \dot{\theta} \right). \quad (9)$$

Therefore

$$F_2 = \{\rho f_m \pi (b^2 - a^2) z_0 + \rho f_m \pi r \sin \theta [b^2 - (a^2 \cos^2 \theta)]\} r \ddot{\theta} + \rho f_m r \pi \cos \theta \{b^2 + [a^2 (\sin^2 \theta - \cos^2 \theta)]\} r \dot{\theta}^2. \quad (10)$$

Consider that

$$P_1 = (b^2 - a^2) z_0 + r \sin \theta [b^2 - (a^2 \cos^2 \theta)],$$

$$P_2 = r \dot{\theta}^2 \cos \theta \{b^2 + [a^2 (\sin^2 \theta - \cos^2 \theta)]\}$$

and

$$S = \rho f_m r \pi.$$

However, we have that  $F_1 = F_2$ ; then

$$\ddot{\theta} = \left( \frac{F_1}{S} - P_2 \right) / P_1. \quad (11)$$

Once the angular acceleration, the angular velocity and the angle of motion have been calculated, the plasma radial velocity  $dr_p/dt$  can be obtained from

$$\frac{dr_p}{dt} = r \dot{\theta} \sin \theta. \quad (12)$$

Hence the sheath position  $r_p$  can also be calculated by using the linear approximation that was used in the axial phase. The axial velocity is

$$\frac{dz_f}{dt} = r \dot{\theta} \cos \theta. \quad (13)$$

### 2.2.1 Circuit and current equations.

$$\frac{d}{dt}[(L_0 + L_T)If_c] + r_0 I = V_0 - \int \frac{I dt}{C_0}; \quad (14)$$

then

$$\frac{dI}{dt} = \left( V_0 - \frac{\int I dt}{C_0} - r_0 I - If_c \frac{dL_r}{dt} \right) / (L_0 + L_T f_c),$$

where

$$\frac{dL_r}{dt} = \frac{\mu \{ (dz_f/dt) \ln[b/(r \cos \theta)] + z_f \dot{\theta} \tan \theta \}}{2\pi}. \quad (15)$$

The voltage across the input terminals of the focus tube can be calculated from

$$V = \frac{d}{dt}(L_T I) = I \frac{dL_r}{dt} + L_T \frac{dI}{dt}. \quad (16)$$

**2.2.2 Motion of the shock wave.** In the slug model, which is suitable for modelling a plasma focus, the magnetic pressure drives a shock wave, creating a space for the current sheath of the magnetic piston to move into, as shown in figure 4. The speed of the magnetic piston can be determined by the first law of thermodynamics applied to an effective increase in the volume between the shock front and the current sheath, created by incremental motion of the shock front [5]. From the shock wave theory, the shock pressure is given by [4]

$$P = G \rho_0 v_s^2, \quad G = \frac{2}{\gamma + 1}, \quad (17)$$

where  $\gamma$  is the specific heat ratio.

The shock wave speed  $v_s$  in an ambient gas of density  $\rho_0$  increases the pressure of the shocked gas (just behind the shock front) to a value  $P$ . If we assume that this pressure is

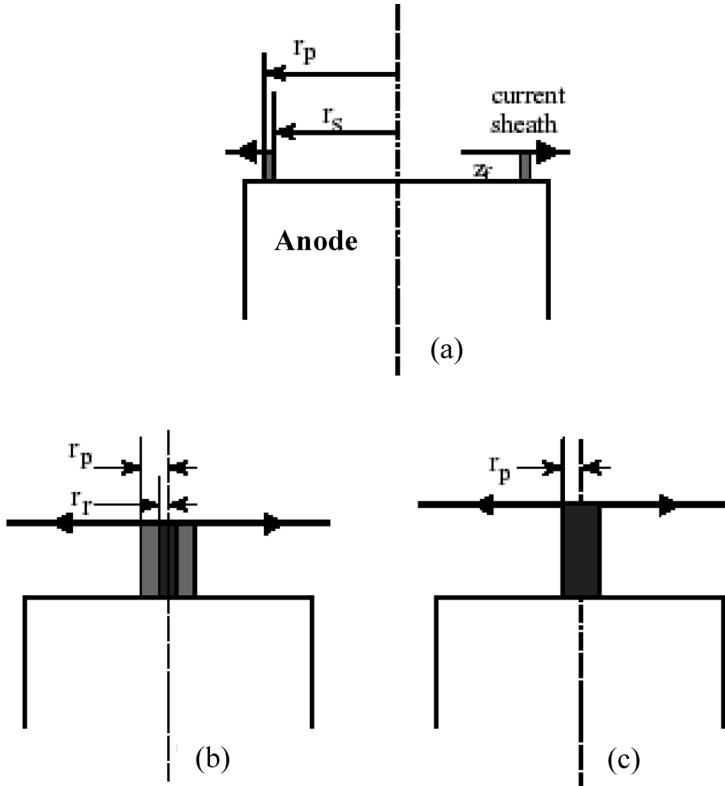


Figure 4. Motions of the piston and shock wave in the radial phase.

uniform from the shock front to the current sheath across the piston, then one may apply  $P = P_m$ , where

$$P_m = \frac{[\mu I_c / (2\pi r \cos \theta)]^2}{2\mu} \quad (18)$$

Thus, from equations (16) and (17), one can obtain [5]

$$v_s = \frac{dr_s}{dt} = \frac{I_c}{2\pi r \cos \theta} - \left( \frac{\mu(\gamma + 1)}{2G\rho_0 f_m} \right)^{1/2} \quad (19)$$

where  $\rho_0 f_m$  is the effective mass density in the slug.

The formation of a stabilized shock wave depends mainly on the discharge conditions, and especially on the initial rate of current increase [24]. In particular, for a shock tube of large radius ratio, the magnetic pressure  $B^2/2\mu$  may decrease by orders of magnitude across the annulus and, thus, it cannot be balanced by the dynamic pressure  $\rho v_s^2$  associated with a propagating planar shock wave [23].

The last equation is also not accurate since, even though the plasma inertia is small, it has an effect on the plasma motion especially if the current decreases and approaches zero. The dependence of the velocity on the current may also not be suitable in all cases, *e.g.* the motion of the shock wave of a non-electric fluid or a body with a velocity higher than the sound velocity. The propagation of the shock wave depends on the fluid velocity. So, one has to calculate the shock wave velocity depending on the plasma velocity in the radial phase; hence we start to find the plasma velocity as a first step.

An adiabatic relationship is assumed for a fixed mass of the gas in the slug during the incremental motion  $dr_s$ . Hence

$$PV^\gamma = \text{constant} \quad (20)$$

and

$$\frac{\gamma dV}{V} + \frac{dP}{P} = 0, \quad (21)$$

where the slug pressure is  $P \propto v_s^2$ ; then

$$\frac{dP}{P} = \frac{2dv_s}{v_s}. \quad (22)$$

Now the slug volume  $V$  is related to the piston radius  $r_p$  and the shock wave radius  $r_s$  by the relationship

$$V = \pi (r_p^2 - r_s^2) z_f, \quad (23)$$

and, at first sight,  $dV = 2\pi(r_p dr_p - r_s dr_s)z_f + \pi(r_p^2 - r_s^2)dz_f$  has to be corrected.

Since it is observed that the motion of the piston,  $dr_p$ , does not change the mass of the gas in the slug, it is considered that the motion of the shock front,  $dr_s$ , causes some amount of the ambient gas to sweep. This swept-up gas is compressed by the ratio  $(\gamma + 1)/(\gamma - 1)$  and will occupy a part of the increased volume  $dV$  [5].

An actual increase in the volume of the original mass of the gas does not correspond to the increment  $dr_s$ , but it does correspond to the effective (reduced) increment  $dr_s[2/(\gamma + 1)]$  [5]. Hence

$$dV = 2\pi \left( r_p dr_p - \frac{2}{\gamma + 1} r_s dr_s \right) z_f + \pi (r_p^2 - r_s^2) dz_f; \quad (24)$$

by substituting equations (24) and (22) into equation (21), we have

$$\frac{2\gamma \{ r_p dr_p - [2/(\gamma + 1)] r_s dr_s \} z_f + \gamma (r_p^2 - r_s^2) dz_f}{z_f (r_p^2 - r_s^2)} + 2 \frac{dv_s}{v_s} = 0 \quad (25)$$

or

$$\frac{d^2 r_s}{dt^2} = \frac{dv_s}{dt} = \frac{2\gamma v_s \{ [2/(\gamma + 1)] r_s (dr_s/dt) - r_p (dr_p/dt) \} z_f - \gamma v_s (r_p^2 - r_s^2) (dz_f/dt)}{2z_f (r_p^2 - r_s^2)}. \quad (26)$$

Hence the axial shock wave propagates in the  $z$  direction towards the axis of the downstream anode until the wave reaches the anode, where the third phase will begin (which is the suitable phase for X-ray production [25]). Figure 5 shows the variations in the radial motion in the radial phase (the second, third, fourth and fifth phases).

**2.2.3 Temperature.** From the shock wave relation the plasma temperature  $T$  is given as [6, 26]

$$T = \frac{M}{R_0 D} \frac{2(\gamma - 1)}{(\gamma + 1)^2} \left( \frac{dr_s}{dt} \right)^2, \quad (27)$$

where  $M$  is the molecule weight and  $D$  is the departure coefficient equal to  $D_N(1 + Z)$  ( $D_N$  is the dissociation number and  $Z$  is the effective charge of the plasma; for example, for deuterium,  $D_N = 2$  whereas, for argon,  $D_N = 1$ ).

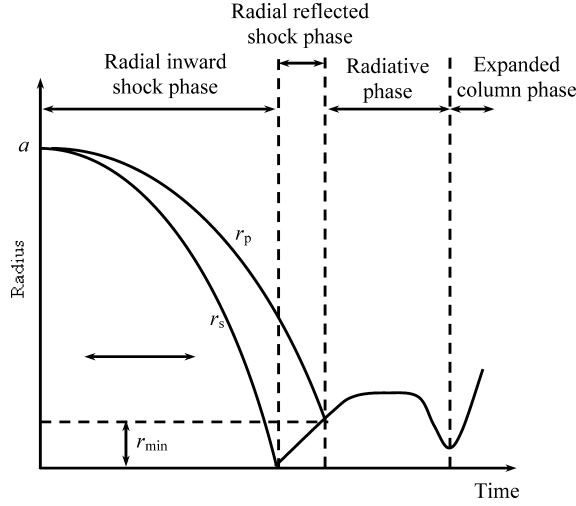


Figure 5. Diagram of the radial piston and shock wave velocities in the radial phase.

The temperature  $T$  may also be calculated as [14, 27]

$$T = \frac{\mu}{8\pi^2 k} \frac{I^2 f_c^2}{DN_0 r^2 f_{mr}}. \quad (28)$$

However, the dependence of the temperature on the current  $I$  may lead us to differentiate between two groups of plasma temperatures according to their dependence on the shock wave velocity or the current. The necessary condition allowing this equation to be used is that the magnetic pressure  $P_m$  due to the  $\mathbf{J} \times \mathbf{B}$  force should exceed the plasma pressure  $P$ . When the magnetic pressure and the plasma pressure are equal, the plasma is in the quasiequilibrium state; then

$$P_m = \frac{B^2}{2\mu}, \quad B = \frac{\mu I f_c}{2\pi r}, \quad P = NkT, \quad P = G\rho_0 v_s^2, \quad G = \frac{2}{\gamma + 1}.$$

So, to calculate the temperature  $T$ , it is necessary to equate  $P$  with  $P_m$ . However, if the  $P_m$  value begins to decrease owing to a high decrement of the current near zero, the equilibrium is not established and one cannot use equation (28); hence the equation to be used is equation (27).

**2.2.4 Computational procedure.** The initial conditions are, at  $t = 0$ ,

$$\theta = 0, \quad \dot{\theta} = \frac{v}{r} = \frac{1}{r} \frac{dz}{dt}, \quad I = I_a, \quad \int I dt = \int I_a dt, \quad \frac{dI}{dt} = \frac{dI_a}{dt}, \quad z_f = 0, \\ \ddot{\theta} = \frac{1}{r} \frac{d^2 z}{dt^2}.$$

Set the time increment to be  $D$  and the incremental time to be  $t = t + D$ , where  $I_a$  is the final current value in the axial phase.

Next the step values are calculated by using the following linear approximations:

$$\begin{aligned}\frac{d\theta}{dt} &= \frac{d\theta}{dt} + \frac{d^2\theta}{dt^2} D, & \theta &= \theta + \frac{d\theta}{dt} D, \\ r_s &= r_s + \frac{dr_s}{dt} D, & z_f &= z_f + \frac{dz_f}{dt} D, \\ I &= I + \frac{dI}{dt} D, & \int I dt &= \int I dt + ID.\end{aligned}\quad (29)$$

By increasing the time and by repeating the calculations of the next step, new values of the parameters will be obtained. The procedure continues until  $r_s/a < \pi/2$ , i.e.  $\cos(r_s/a) < 0$ .

### 2.3 Radial reflected shock phase

In this phase, when the shock wave has reached the axis, the piston can move towards the axis by assuming a virtual forward shock front moving with the 'on-axis' speed of an incident shock. The reflected shock wave travels outwards with a fraction of the on-axis incident shock speed, which may be taken to be 0.3. The equations in this phase are the same as in the previous phase except for the equation for the reflected shock wave speed  $v_{rs}$ , which is

$$v_{rs} = -0.3v_s, \quad (30)$$

where  $v_s$  is the last value in the previous phase (the radial inward shock phase).

#### 2.3.1 Piston speed.

$$\ddot{\theta} = \left( \frac{F_1}{S} - P_2 \right) / P_1 \frac{dr_p}{dt} = r\dot{\theta} \sin \theta. \quad (31)$$

#### 2.3.2 Elongation speed.

$$\frac{dz_f}{dt} = r\dot{\theta} \cos \theta. \quad (32)$$

#### 2.3.3 Circuit equation.

$$\frac{dI}{dt} = \left( V_0 - \frac{\int I dt}{C_0} - r_0 I - I f_c \frac{dL_r}{dt} \right) / (L_0 + L_T f_c), \quad (33)$$

#### 2.3.4 Tube voltage.

$$V = \frac{d}{dt} (L_T I) = I \frac{dL_r}{dt} + L_T \frac{dI}{dt}. \quad (34)$$

#### 2.3.5 Plasma inductance.

$$L_r = \frac{\mu f_c z_f \ln [b / (r \cos \theta)]}{2\pi}. \quad (35)$$

**2.3.6 Plasma temperature.** Similar to the last value in the previous phase (the radial inward shock phase), the plasma temperature is still constant in this phase, as the shock wave velocity is constant.

Continue the procedure until  $r_{\text{rs}} \geq a \cos \theta$ .

## 2.4 Radiative phase

The radiative phase begins when the reflected shock wave has reached the piston current sheath. In this phase, the plasma gains some energy by Joule heating and loses energy through Bremsstrahlung radiation and line radiation [10, 11].

The Joule heating term is obtained by using the Spitzer form of resistivity for the plasma column:

$$\frac{dQ_J}{dt} = R I^2 f_c^2, \quad (36)$$

where

$$R = \frac{1290 Z z_f}{\pi a^2 \cos^2 \theta T^{3/2}}.$$

The Bremsstrahlung loss term may be written as

$$\frac{dQ_B}{dt} = -1.6 \times 10^{-40} N_i^2 (\pi a^2 \cos^2 \theta) z_f T^{1/2} z^3, \quad (37)$$

where

$$N_0 = 6 \times 10^{26} \frac{\rho_0}{M}, \quad N_i = N_0 f_{\text{mr}} \left( \frac{a}{r \cos \theta} \right)^2. \quad (38)$$

The line loss term may be written as

$$\frac{dQ_L}{dt} = - \frac{4.6 \times 10^{-31} N_i^2 Z Z_n^4 (\pi a^2 \cos^2 \theta) z_f}{T} \quad (39)$$

and

$$\frac{dQ_T}{dt} = \frac{dQ_J}{dt} + \frac{dQ_B}{dt} + \frac{dQ_L}{dt}. \quad (40)$$

$dQ_T/dt$  is the total power gain or loss of the plasma column and  $Z_N$  is the atomic number of the gas used.

The resultant total power  $dQ_T/dt$  has to be inserted carefully into the equation of motion. It is very important that the expansion process that may occur during the radial phase is explained. However, the introduction of the power equations into the model leads to many changes in the entire model behaviour, such as an abrupt change in the current and voltage waveforms to undesirable values and sometimes oscillatory values of the current, voltage, temperature, radial velocity and position.

Hence, it may be suitable now to calculate the energy terms without inserting them into the main equation. In order to avoid the errors that can be made, we think that the energy terms must be inserted from the beginning of the radial phase, which also emits radiation, although of lower level. Hence, it will make gradual changes.

**2.4.1 Temperature.** Equation (27) is used, where the shock wave velocity term  $dr_s/dt$  is dropped in this phase. So the temperature equation (28) of the plasma pressure equilibrium can also be used. The attempts made to utilize this equation in both models showed a very large

discrepancy between the calculated and the experimental values in both models. It should also be noted that the column radius decrement as a result of the magnetic pressure affect is compensated by an increment in the column length. Another disadvantage is that most of measurements were carried out before the plasma has reached this phase. The temperature in this phase needs further careful study. The same equations that have been previously used to calculated changes in the speed, current and voltage are used here except for  $v_{rs}$ , which is not calculated now.

#### 2.4.2 Piston speed.

$$\frac{d\theta}{dt} = \frac{d\theta}{dt} + \frac{d^2\theta}{dt^2}D, \quad (41)$$

$$\frac{dr_p}{dt} = r\dot{\theta} \sin \theta.$$

#### 2.4.3 Elongation speed.

$$\frac{dz_f}{dt} = r\dot{\theta} \cos \theta. \quad (42)$$

#### 2.4.4 Circuit equation.

$$\frac{dI}{dt} = \left( V_0 - \frac{\int I dt}{C_0} - r_0 I - I f_c \frac{dL_r}{dt} \right) / (L_0 + L_T f_c). \quad (43)$$

#### 2.4.5 Tube voltage.

$$V = \frac{d}{dt}(L_T I) = I \frac{dL_r}{dt} + L_T \frac{dI}{dt}. \quad (44)$$

#### 2.4.6 Plasma inductance.

$$L_r = \frac{\mu f_c z_f \ln [b/(r \cos \theta)]}{2\pi}. \quad (45)$$

To avoid the singularity of the snowplough model, the procedure will continue until a chosen value ( $\cos \theta \leq 0.05$ ).

### 2.5 Expanded column axial phase

The equation is the same as was used in the axial phase except that the plasma inductance  $L$  is given by

$$L = L_a = \frac{\mu}{2\pi} (\ln c) + L_r, \quad (46)$$

and

$$L_r = \frac{\phi_r}{I} = \frac{\mu(r\theta + z_0) \ln c}{2\pi \cos \theta}$$

is equal to the last value in the previous fourth phase (the radiative phase). Continue the procedure until the discharge time  $t$  exceeds half the periodic time  $t_0$ , i.e.  $t > \pi(L_0 C_0)^{1/2}$ .

### 3. Comparison between our model and the experimental results

In order to verify our model, a comparison between theoretical and experimental results was made. Table 1 show the parameters of some plasma focus devices, which were used in the comparison. The simulation code is written in Basic language under Microsoft Excel.

The following comparison is made to verify the model in the radial phase, since the main change in our model occurs only in the radial phase. Additional information about the comparisons made in the axial phase using the same idea as the Lee model can be found in [9, 2, 14], and by using other models in [3, 16, 34, 35].

#### 3.1 Discharge current and voltage in the radial phase

In most cases, the discharge currents calculated by the Lee model and our model are similar in their behaviour and values to each other and to the discharge current obtained by experiment. Figure 6 shows an example of the experimental discharge current obtained by Moreno *et al.* [28] and discharge currents calculated by using theoretical models.

The greatest difference appears in the value of the spike voltage. Figure 7 shows the discharge voltage obtained experimentally by Liu *et al.* [25], and the discharge voltage calculated by using theoretical models.

Figure 8 shows a comparison between the data calculated by using two theoretical models and the experimental data obtained for different plasma focus devices. It can be seen that in most cases the results obtained by using our model show good agreement with the values found by experiment.

Table 1. Some plasma focus devices and their parameters.

Reference	$L_0$ (nH)	$C_0$ ( $\mu$ F)	$b$ (cm)	$a$ (cm)	$Z$ (cm)	$r_0$ ( $\Omega$ )	$V_0$ (kV)	$P_0$ (Torr)	Gas used
[25]	110	30	3.2	0.95	16.3	0.012	13	1.3–2.9	Ne
[14]	39	10.5	4.225	1.9	8.71	0.01	30	1.5–4.5	D <sub>2</sub>
[28]	65	0.160	1.05	0.8	1	0.6	25	0.35	H <sub>2</sub>
[29]	16	90	5	2.5	20	0.0033	17.3	13.84	D <sub>2</sub>
[30]	9	1000	7.55	5	33	0.009	25	3.67	H <sub>2</sub>
[31]	38	0.88	1.55	0.6	2.8	0	28	6.53	D <sub>2</sub>
[32]	8.9	1332	18.4	12.2	60	0.0026	39	2	D <sub>2</sub>
[33]	58	28	3.2	0.95	16.3	0.012	14	1.5	Ar

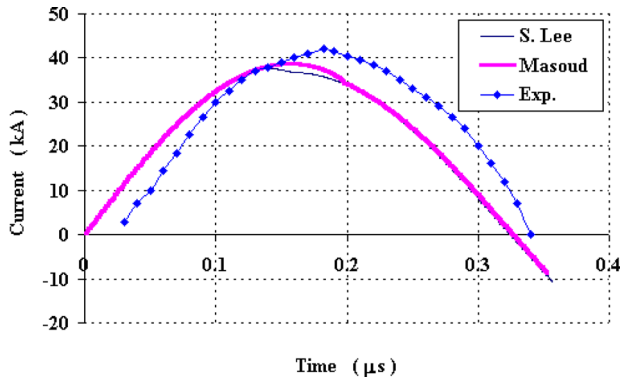


Figure 6. Discharge current as a function of the discharge time according to Moreno *et al.* [28].

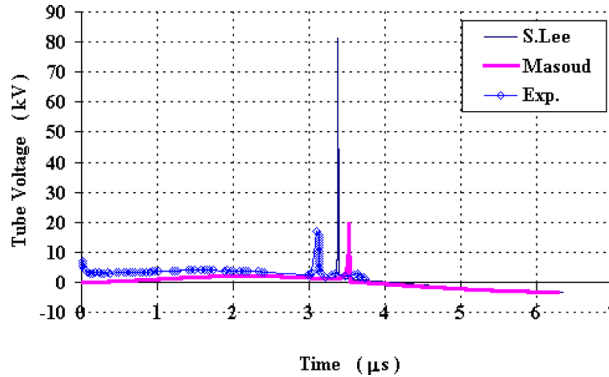


Figure 7. Tube voltage as a function of the discharge time according to Liu *et al.* [25].

### 3.2 Current sheath elongation

According to Kasperczuk *et al.* [32], the plasma column will be formed during the last 250 ns. On expiration of this time moment, a plasma column of about 12 cm length should have been formed. This result agrees with the result obtained by our model, in which the elongation speed of the plasma column does not change so much during the last 250 ns with the variation in its length from 11 to 12.2 cm, whereas in the Lee model the elongation length varies between 8.4 and 14.1 cm during the last 250 ns.

According to Moreno *et al.* [28], the elongation speed is about  $0.45 \mu\text{s cm}^{-1}$  in the middle of the process of column formation and at the end of it, which means that this speed is much higher at the beginning of the process.

That result shows good agreement with the result obtained by using our model, which estimates the decrement of the elongation speed with time.

Figure 9 shows a comparison between the column lengths obtained by experiment and the column lengths calculated by using theoretical models.

### 3.3 Radial phase velocity

A comparison between the values of the radial piston speed obtained by using two theoretical models and its values obtained by experiment is shown in figure 10. From the figure it can

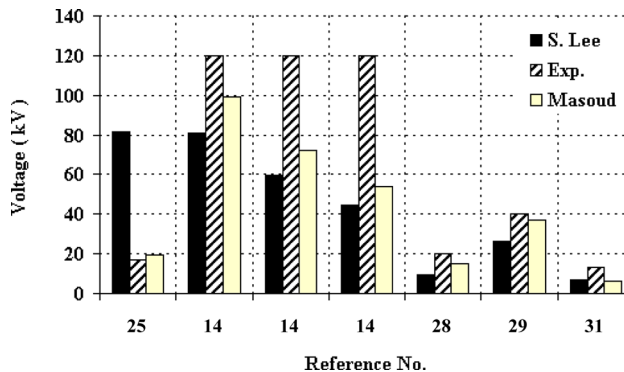


Figure 8. Voltage spike values in different references.

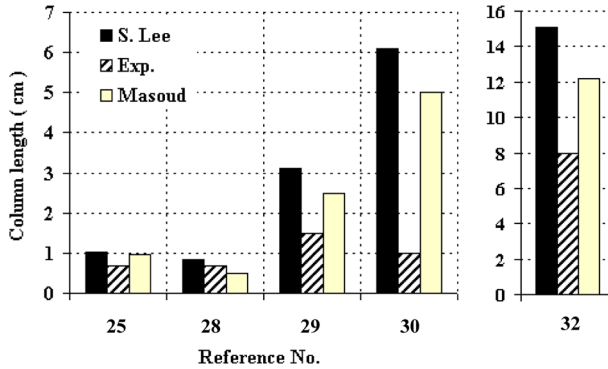


Figure 9. Column length values in different references.

be seen that our model shows better agreement with the experimental data than the Lee model does.

Figures 11 and 12 show examples of the variations in the radial position and speed respectively with time obtained according to Moreno *et al.* [28], and figures 13 and 14 show examples of the variations in the radial position and speed respectively with time obtained according to

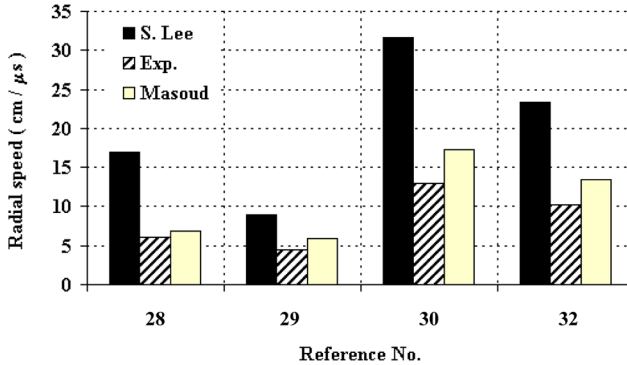


Figure 10. Radial speed values in different references.

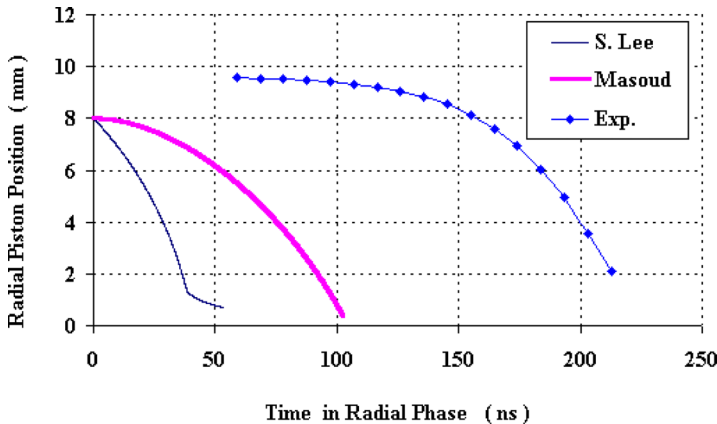


Figure 11. Radial position as a function of the radial phase time according to Moreno *et al.* [28].

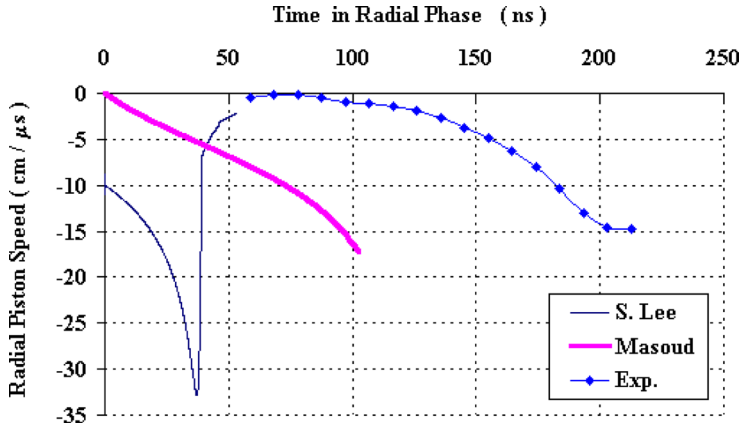


Figure 12. Radial speed as a function of the radial phase time according to Moreno *et al.* [28].

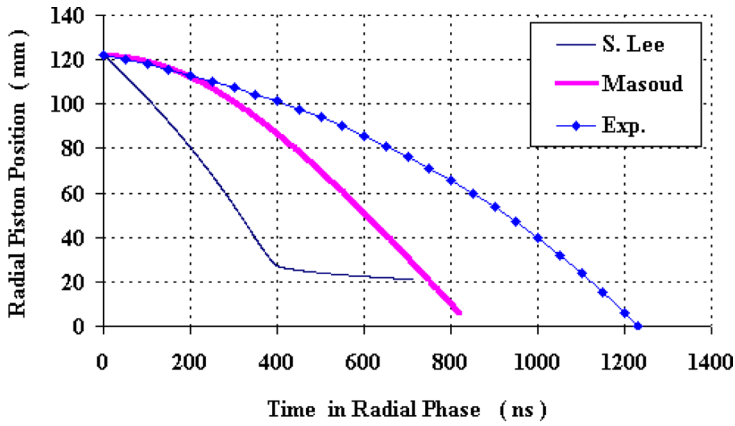


Figure 13. Radial position as a function of the radial phase time according to Kasperczuk *et al.* [32].

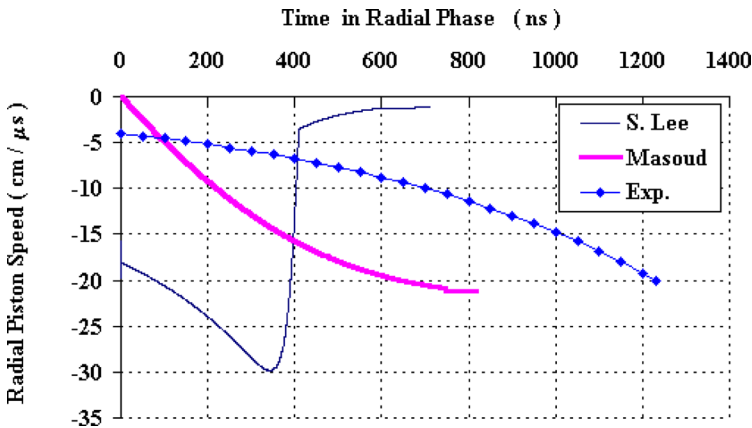


Figure 14. Radial speed as a function of the radial phase time according to Kasperczuk *et al.* [32].

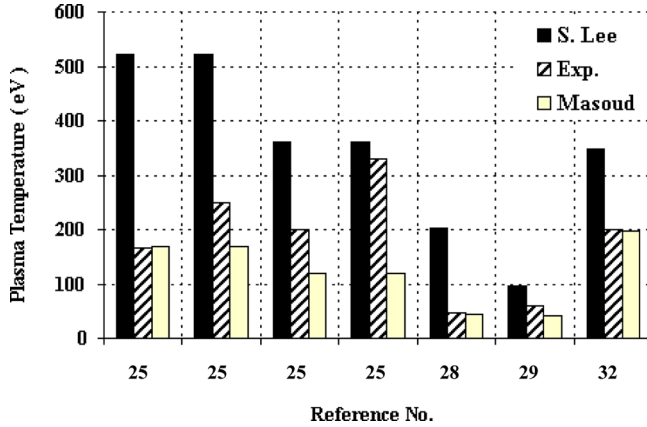


Figure 15. Plasma temperature values in different references.

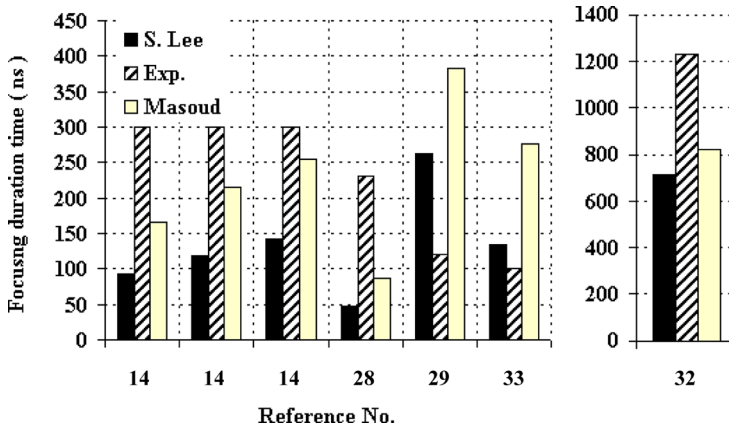


Figure 16. Focusing time duration values in different references.

Kasperczuk *et al.* [32]. It can be seen that our new model gives a better approximation to the experiments with respect to the behaviour and values.

### 3.4 Plasma temperature

Figure 15 shows a comparison between the two theoretical models and the values of the plasma temperature obtained by experiment. It can be seen that our model shows better agreement with the experimental data than the previous Lee model does.

A comparison between the two theoretical models and the values of the radial phase time duration obtained by experiment is shown in figure 16. This figure shows some differences between the two models by comparing their results with the obtained experimental data.

## 4. Conclusion

This model depends on the continuity between the plasma velocity in the axial phase and the plasma velocity in the radial phase. In the axial phase, the snowplough model was applied to

plasma sheath motion similar to the Lee model. Two equations were used during this phase: the equation of motion, which depends on the rate of the momentum change, and the circuit equation. By solving these two equations, we obtained values of the axial sheath velocity, the axial position, the plasma inductance, the discharge current and the discharge voltage.

In the radial phase, it is suggested that the motion of the plasma sheath will be spherical in shape depending on the snowplough model rather than the slug model to keep the continuity of the plasma sheath motion between the axial and radial phases. One could see that the angle of motion was inserted into all equations.

After the plasma sheath position and velocity had been calculated numerically by using previous equations, the slug model was used to calculate the shock wave velocity. Then, the electron temperature could be calculated.

From the results of numerical calculations we obtained the values of the discharge current, the axial speed, the axial position, the spike voltage, the radial piston speed, the radial piston position, the plasma column length and the plasma temperature.

The comparison of the calculated values with the values obtained by experiment by other researchers showed good agreement. On this basis we concluded that this model is the most suitable model for describing a plasma focus device.

## References

- [1] J. Salge. Developments in plasma focus research. In *Proceedings of the 2nd Workshop on Plasma and Laser Technology, International Cooperation Bilateral Seminar*, Vol. 2, Cairo, Egypt, 1990 (Forschungszentrum Jülich, Jülich, 1990), p. 349.
- [2] M. Mathuthu, T.G. Zengeni and A.V. Gholap. The three-phase theory for plasma focus devices. *IEEE Trans. Plasma Sci.*, **25**, 1382 (1997).
- [3] S. Maxon and J. Eddleman. Two-dimensional magnetohydrodynamic calculations of the plasma focus. *Phys. Fluids*, **21**, 1856 (1978).
- [4] D.E. Potter. The formation of high density z-pinch. *Nucl. Fusion*, **18**, 813 (1978).
- [5] S. Lee. Technology of the plasma focus. In *Proceedings of the 1st Tropical College on Applied Physics: Laser and Plasma Technology*, Kuala Lumpur, Malaysia, 1984 (World Scientific, Singapore, 1985), p. 387.
- [6] S. Lee. Electronic shock tube. In *Proceedings of the 1st Tropical College on Applied Physics: Laser and Plasma Technology*, Kuala Lumpur, Malaysia, 1984 (World Scientific, Singapore, 1985), p. 3.
- [7] S. Lee. Plasma focus experiment. In *Proceedings of the 1st Tropical College on Applied Physics: Laser and Plasma Technology*, Kuala Lumpur, Malaysia, 1984 (World Scientific, Singapore, 1985), p. 37.
- [8] S. Lee, C.S. Wong, T.Y. Tou, et al. Computation of dynamics of pulsed plasmas. In *Proceedings of the 1st Tropical College on Applied Physics: Laser and Plasma Technology*, Kuala Lumpur, Malaysia, 1984 (World Scientific, Singapore, 1985), p. 63.
- [9] S. Lee. A sequential plasma focus. *IEEE Trans. Plasma Sci.*, **19**, 912 (1991).
- [10] B. Shan, P. Lee and S. Lee. Improving energy efficiency of plasma focus. *Sing. J. Phys.*, **16**, 25 (2000).
- [11] M.H. Liu and S. Lee. SXR radiation modelling for neon plasma focus. In *Proceedings of the 1998 International Congress on Plasma Physics and the 25th EPS Conference on Controlled Fusion and Plasma Physics*, European Conference Abstracts, Vol. 22C, Prague, Czech Republic, 29 June–3 July 1998 (European Physical Society, Geneva, 1998), p. 2169.
- [12] S. Lee and A. Serban. Dimensions and lifetime of the plasma focus pinch. *IEEE Trans. Plasma Sci.*, **24**, 1101 (1996).
- [13] S. Lee. Application of energy balance to compute plasma pinch ratios. *J. Appl. Phys.*, **54**, 3603 (1983).
- [14] M. Zakauallah, T.J. Baig and G. Murtaza. Numerical design of plasma focus optimization. In *Proceedings of the Symposium on Small Plasma Physics Experiments*, Trieste, Italy, 1987 (World Scientific, Singapore, 1987), p. 23.
- [15] C. Moreno, F. Casanova, G. Correa, et al. Experimental study and two-dimensional modelling of the plasma dynamics of magnetically driven shock waves in a coaxial tube. *Plasma Phys. Controlled Fusion*, **45**, 1989 (2003).
- [16] Z. Shen, C. Liu, C. Lee, et al. A study of a coaxial plasma gun. *J. Phys. D: Appl. Phys.*, **28**, 314 (1995).
- [17] N.F. Tsagas, G.L.R. Mair and A.E. Prinn. Motion and shape of snowplough sheets in coaxial accelerators. *J. Phys. D: Appl. Phys.*, **11**, 1263 (1978).
- [18] L.C. Burkhardt and R.H. Lovberg. Current sheet in a coaxial plasma gun. *Phys. Fluids*, **5**, 341 (1962).
- [19] S.P. Chow, S. Lee and B.C. Tan. Current sheath studies in a coaxial plasma focus gun. *J. Plasma Phys.*, **8**, 21 (1971).
- [20] F.J. Fishman and H. Petschek. Flow model for large radius-ratio magnetic annular shock-tube operation. *Phys. Fluids*, **5**, 632 (1962).

- [21] M. Rabinski and K. Zdunek. Computer simulations and experimental results in studies of plasma dynamics during IPD process. *Surf. Coat. Technol.*, **116–119**, 679 (1999).
- [22] M. Rabinski and K. Zdunek. Physical model of dynamic phenomena in impulse plasma coaxial accelerator. *Vacuum*, **48**, 715 (1997).
- [23] J.C. Keck. Current distribution in a magnetic annular shock tube. *Phys. Fluids*, **5**, 630 (1962).
- [24] C.T. Chang. Shock wave phenomena in coaxial plasma guns. *Phys. Fluids*, **4**, 1085, (1961).
- [25] M. Liu, X. Feng, S.V. Springham, *et al.* Soft X-ray yield measurement in a small plasma focus operated in neon. *IEEE Trans. Plasma Sci.*, **26**, 135 (1998).
- [26] K.H. Kwek, T.Y. Tou and S. Lee. Current sheath structure of the plasma focus in the run-down phase. *IEEE Trans. Plasma Sci.*, **18**, 826 (1990).
- [27] V.S. Komel'kov and V.I. Modzolevskii. Coaxial accelerator for dense plasmas. *Soviet J. Plasma Phys.*, **3**, 533 (1977).
- [28] J. Moreno, P. Silva and L. Soto. Optical observations of the plasma motion in a fast plasma focus operating at 50 J. *Plasma Sources Sci. Technol.*, **12**, 39 (2003).
- [29] J.W. Mather and P.J. Bottoms. Characteristics of the dense plasma focus discharge, *Phys. Fluids*, **11**, 611 (1968).
- [30] M. Scholz, L. Karpinski, W. Stepniewski, *et al.* Foam liner driven by a plasma focus current sheath. *Phys. Lett. A*, **262**, 453 (1999).
- [31] P. Silva, J. Moreno, L. Soto, *et al.* Neutron emission from a fast plasma focus of 400 Joules. *Appl. Phys. Lett.*, **83**, 3269 (2003).
- [32] A. Kasperczuk, R. Kumar, R. Miklaszewski, *et al.* Study of the plasma evolution in the PF-1000 device by means of optical diagnostics. *Physica Scripta*, **65**, 96 (2002).
- [33] W. Usada and Suryadi. BATAN PFFF. In *Proceedings of the Symposium on Small Plasma Physics Experiments*, Trieste, Italy, 1987 (World Scientific, Singapore, 1987), p. 15.
- [34] D. Dietz. Coaxial plasma accelerator in the snowplough model: analytical solution in the weak coupling limit. *J. Appl. Phys.*, **62**, 2669 (1987).
- [35] S.F. Schaer. Coaxial plasma gun in the high density regime and injection into a helical field. *Acta Phys. Polonica A*, **88**, S77 (1995).

